energies

MDPI

Article

Experimental Investigation on the Strength and Failure Behavior of Coal and Synthetic Materials under Plane-Strain Biaxial Compression

Hongwei Zhang [1,2,†], Zhijun Wan [1,*], Dan Ma [3,*,†], Yuan Zhang [1], Jingyi Cheng [1] and Qi Zhang [2,4]

1 Key Laboratory of Deep Coal Resource Mining of Ministry of Education, School of Mines, China University of Mining & Technology, Xuzhou 221116, Jiangsu, China; cumtzhw@gmail.com (H.Z.); zhangyuan@cumt.edu.cn (Y.Z.); Cjycumt@Hotmail.com (J.C.)
2 Department of Energy and Mineral Engineering, EMS Energy Institute, and G3 Center, The Pennsylvania State University, University Park, PA 16802, USA; zhangqi428@126.com
3 School of Resources & Safety Engineering, Central South University, Changsha 410083, Hunan, China
4 State Key Laboratory for Geomechanics and Deep Underground Engineering, China University of Mining & Technology, Xuzhou 221116, Jiangsu, China
* Correspondence: zhjwan@126.com (Z.W.); dan.ma@nottingham.ac.uk (D.M.)
† All authors contributed equally to this work.

Academic Editor: Mehrdad Massoudi
Received: 24 February 2017; Accepted: 1 April 2017; Published: 7 April 2017

Abstract: An evaluation of the failures of coal under variable conditions in relation to the stability of coal pillars is an important issue for coal mining. This paper presents the results of an experimental investigation of the mechanical behavior of brittle coal under plane-strain biaxial stress state (PSBSS) compression. The synthetic specimens were meant to test the ductile properties. Modified surface instability detection apparatus was setup to carry out the tests. The results show that the stress-strain curves of coal and synthetic specimens under the PSBSS can be divided into four typical stages, namely original microcrack closure, elastic deformation, sudden stress drop, and residual behavior. The stress-strain curve of coal under PSBSS compression showed periodic stress drops during the post-peak phase, while the curve of the synthetic specimen presented a moderate decrease during the post-peak stage. The remarkable residual strengths of the coal and composites can be observed using these curves, which is vital to the stability of specimens after the failure strength is exceeded. Strain rates have a significant effect on the strength of coal samples under PSBSS compression. Specifically, a higher strain rate indicates a greater peak strength. The failure modes for coal and synthetic specimens are different. During PSBSS compressive tests, coal showed a split failure under different strain rates. For flexible composites, the failure pattern is conjugate shear failure. The study indicated that the Modified Lade and Modified Wiebols-Cook criteria are competent for estimating the defined strength coefficient, which is a ratio proposed to estimate the PSBSS peak strength.

Keywords: biaxial compression; coal; criterion; peak strength; plane-strain

1. Introduction

Coal is in high demand as a resource for generating electricity in China. To achieve safe mining, deformation and the failure of rocks must be considered [1]. Plane states of strain, where the behavior of intact rock is a concern, are encountered in many types of long structures (e.g., coal pillars) or excavations in continuous rocks [2,3]. However, rocks under a plane-strain biaxial stress state (PSBSS) [4], a special case state of plane strain that corresponds to a biaxial state of stress, is often considered in geotechnical engineering, such as in longwall and highwall mining coal pillars. As shown in Figure 1a–c, a long coal pillar was retained to support the overlying strata in the Baodian coalmine

in eastern China. The layout of the mining area is illustrated in Figure 1b and the 3D schematic of the long pillar is presented in Figure 1c. The long coal pillar between the adjacent working faces (i.e., 6302 and 6301 panels) is ~1000 m in length and the cross-section area of the pillar is 3 m × 3 m. In longwall and highwall coal mining systems, the key is to study the mechanical behavior of the long pillars and prevent their failure. The optimal design of structures is based not only on peak strength, but also on post-peak behavior, and thus, on residual strength [5]. However, research related to PSBSS is typically unavailable, and uniaxial and biaxial stress states are often introduced to estimate the mechanical behavior of these pillars [6–8], which neglects the essential plane-strain biaxial stress state.

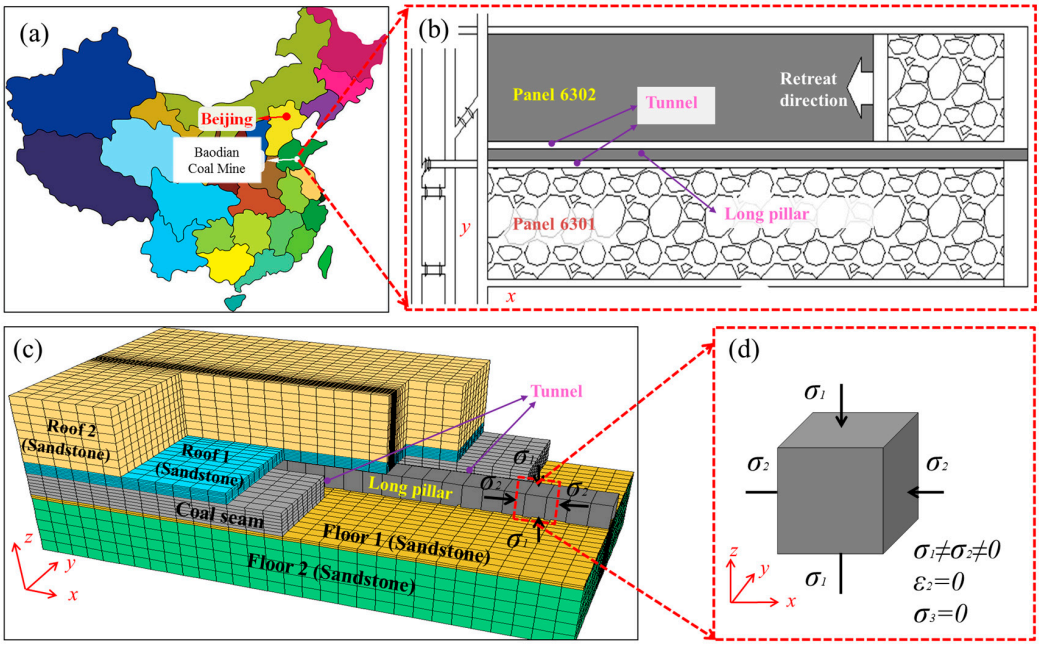

Figure 1. An in situ coal pillar under the PSBSS. (**a**) Baodian coalmine in eastern China; (**b**) Layout of 6302 working face of the Baodian coalmine. A long pillar was retained between the adjacent 6301 and 6302 panels; (**c**) 3D schematic of the long pillar; (**d**) Coal specimen under PSBSS. σ_1 is the vertical stress applied by the overburden, σ_2 is the confined stress applied by adjacent portion of the coal pillar and σ_3 is considered to be zero in this stress state. Specifically, according to the plane strain concept, the principle strain along the longest dimension (ε_2) is zero.

It is well known that the essential notion in the plane strain concept is that the displacement and stress conditions are identical in all planes perpendicular to the long axis of the elastic structure in the infinite medium [9]. As shown in Figure 1b,c, the long coal pillar is under a biaxial stress state in a longwall coal mining system. According to the plane-strain concept, the principal strain (ε_2) in the direction of the longest dimension of the pillar (x-axial) is constrained (i.e., $\varepsilon_2 = 0$). The vertical stress (σ_1) is applied by the overlying strata. σ_2 and σ_3 are the horizontal stresses along the x-axial direction and y-axial direction, respectively. Specifically, the stress along the x-axial direction is not zero (i.e., $\sigma_2 \neq 0$). In addition, there is no stress normal to the free faces after the excavation of tunnels (i.e., $\sigma_3 = 0$) (Figure 1b,c). Therefore, coal blocks in the long coal pillar only suffer from stresses along the x-axial and z-axial directions under the PSBSS (i.e., $\sigma_1 \neq \sigma_2 \neq 0$ and $\sigma_3 = 0$) (Figure 1d).

Since 1969 [10], the fracture evolution and mechanical behaviors of rocks and concretes under biaxial compression have been extensively studied [11–16]. In normal biaxial compression tests, the intermediate principle stress (σ_2) increased proportionally with the maximum principle stress (i.e., $\sigma_1 = d\sigma_2$, where d is a constant between 0.0 and 1.0). Typical failure envelopes of geomaterials in biaxial compression tests indicate that the peak biaxial compression strength increases with the rise of the intermediate principle stress (σ_2) [10,11,14,17–26].

The presence of the intermediate principle stress (i.e., confined stress) (σ_2) can not only affect the failure strength, but also radically change the deformation behaviors of the geomaterials [27–29]. The fracture surface is exactly parallel to the direction of the intermediate principle stress for brittle rocks such as granite, limestone, and dolomite under biaxial compression tests [11]. For ductile materials, such as mortar and sand, a shear failure was always observed [30]. Wang et al. [14] and Lim et al. [29] suggested that the confined stress (i.e., σ_2) can change the failure modes of concrete from the common column type, to the shear type and parallel plate type.

The PSBSS is a special case of the biaxial stress state, in which the intermediate principle strain is zero, and research on rocks or synthetic materials under PSBSS compression is limited. Papamichoes et al. [31] designed plane strain biaxial apparatus to investigate surface spalling phenomena in rocks, indicating a shear-mode failure for brittle rocks under the PSBSS. Tao [32] tested the failure strength of soft and hard coal specimens under the PSBSS and they found that greater failure strengths will appear under the PSBSS than those under a uniaxial stress state, for both kinds of coal specimens. Powrie et al. [33] and Alshibli et al. [34] also found shear failure shapes in Ottawa sand and numerical samples, respectively. Powrie et al. defined this failure pattern of geomaterials under the PSBSS as conjugate shear bands.

In this paper, we tested coal samples (brittle) and synthetic materials (ductile) under PSBSS compression. This research focuses on investigating: (1) the influence of the strain rate on peak strength; (2) the residual behavior under the PSBSS; and (3) the qualified criterion that can estimate the strength parameters, such as peak strength. We begin with a description of the experimental methodology. Then, the results are illustrated and discussed. Finally, we introduce a strength coefficient and conduct a failure criteria study.

2. Experimental Methodology

2.1. Sample Description and Preparation

Coal specimens, obtained by the cutting of large blocks taken from the #3 coal seam at the 6302 longwall panel in the Baodian coalmine, China, were 70.7 × 70.7 × 70.7 mm^3 in size (Figure 2a,b). The coal was a type of bituminous coal with an average unit weight of 1360 kg/m^3. The specimens were carefully surfaced using a rotating grinding device.

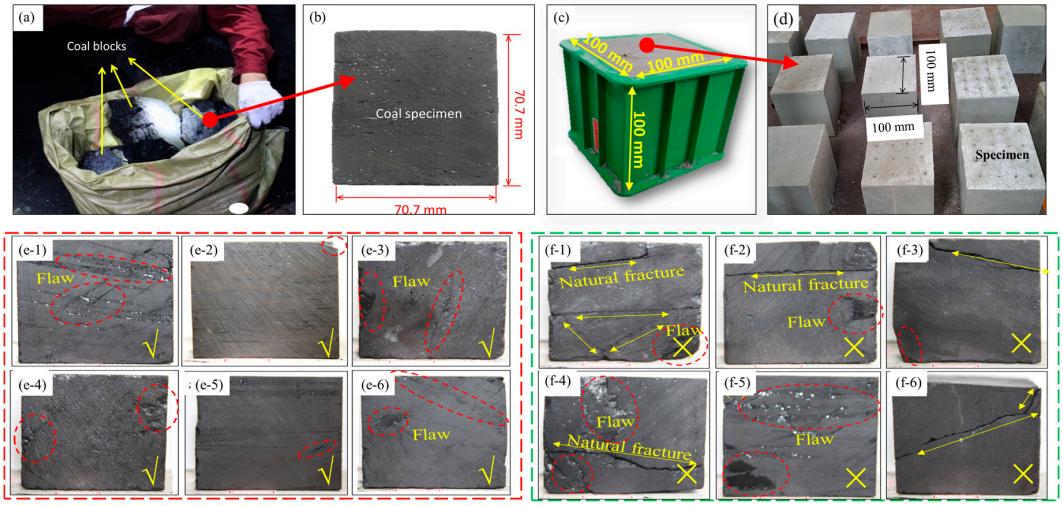

Figure 2. Coal blocks and specimens. (**a**) Coal blocks which are taken from the in situ working face at a depth of approximately 450 m and are processed into cube specimens; (**b**) Coal specimen (70.7 × 70.7 × 70.7 mm^3 in size); (**c**) Synthetic specimen (100 × 100 × 100 mm^3 in size) in a mould; (**d**) Synthetic specimens; (**e-1**–**e-6**) Typical coal specimens that were employed in this study; (**f-1**–**f-6**) Coal specimens that contained large fractures and flaws were abandoned to minimize experimental error.

Synthetic materials were prepared by scaling the geometrical, physical, and mechanical parameters (e.g., size, density, and strength) of the in situ coal pillar (cross area 3 × 3 m^2) under the specific PSBSS [35]. These rock-like specimens (Figure 2c,d) were 100 × 100 × 100 mm^3 cube blocks and were encased by cemented sand and plaster. All of the synthetic specimens were prepared by a plastic vessel to assure homogeneity along the axis and parallelism of the end surfaces. The weight ratio of sand, cement, and plaster for the synthetic specimens was 20:9:21. The specimen number and test conditions are shown in Table 1.

It should be noted that natural fractures and flaws in coal specimens could affect the failure strength and deformation of coal, which may increase the experimental uncertainty. Above 30 samples were prepared to conduct the test. However, due to coal blocks containing fractures and flaws, it was difficult to cut them into intact rocks. Furthermore, the formation of natural flaws in these samples was unavoidable during the cutting process. To decrease the experimental error, relatively intact coal samples were carefully selected. As shown in Figure 2(e-1–e-6), coal specimens containing the smallest fractures and lowest number of flaws were employed in this study, while specimens containing large fractures and huge flaws (Figure 2(f-1–f-6)) were abandoned.

Table 1. Test conditions of specimens.

Material	Test Method	Strain Rate (10^{-4}/s)	Number
Coal	PSBSS	2.4	6
		5.0	7
		9.5	4
Synthetic material	PSBSS	2.4	5

2.2. Experimental Apparatus and Procedures for the PSBSS Tests

To achieve the PSBSS, we designed a suit of apparatus. The apparatus was modified from a Surface Instability Detection Apparatus that was employed to investigate the surface spalling instabilities of rocks [21,24,31,36], rock bursting experiments on coal, and constitutive behavior in plane strain [25,30]. In this apparatus (Figure 3a), a cube or prismatic specimen, placed between two rigid vertical sidewalls, was subjected to an axial load applied through the platens. The adjustable wall, which was used to test specimens with a different size, was bolted to prevent lateral deflection, and compression stress (σ_1) was applied using a testing system. In particular, lube oil was used to minimize fraction at the interface during experimentation.

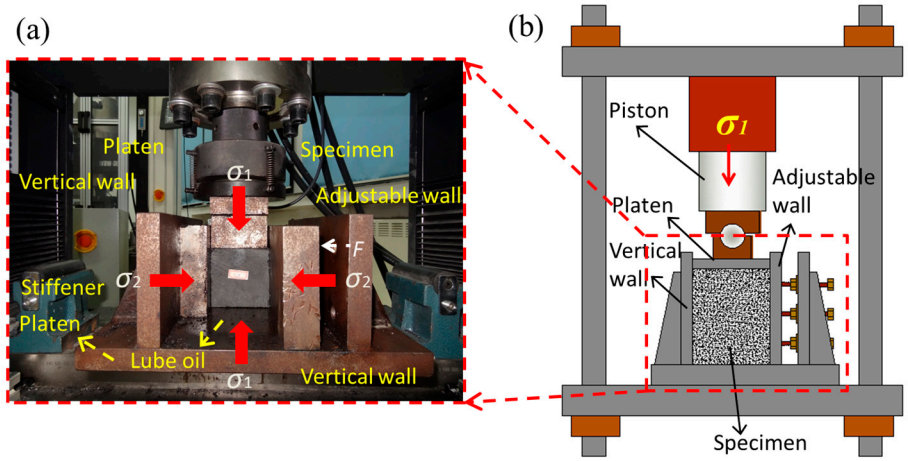

Figure 3. PSBSS compression test system. (**a**) Photograph of the apparatus; (**b**) Schematic of the test system.

The PSBSS compression experiments were carried out on a rock servo-controlled system, with a maximum loading capacity of 300 kN and a maximum displacement resolution of 0.001 mm (Figure 3b). This servo-controlled system can test samples in load (stress) or displacement (strain) control. Specifically, the strain control rates for the coal specimens were set at 2.4×10^{-4}/s, 5.0×10^{-4}/s, and 9.5×10^{-4}/s, while the rate for the synthetic materials was 2.4×10^{-4}/s (Table 1).

The tests were performed through the following procedures: (1) Place a specimen on a lower loading platen; (2) Use screws to provide a reactive force (F) for the adjustable wall, until the specimen is perfectly confined; (3) Put the top-loading platen on the specimen, through which the axial load (σ_1) is applied. Note that the length of this platen (a_1) is slightly smaller than the length of the specimen (a_2) that allows a width tolerance of approximately +1.0 mm between adjustable walls and loading platens; (4) Compress the top plate at a specific strain control rate until the failure takes place, and during the whole PSBSS compression experiments, the loads are recorded simultaneously.

3. Results and Discussion

3.1. Mechanical and Deformation Behavior of Coal Specimens under PSBSS Compression

3.1.1. Stress-strain Curves of Coal Specimens

Typical PSBSS stress-strain curves for coal under different strain rates are presented in Figure 4. The axial stress-axial strain behavior of coal under the PSBSS can be approximately divided into four typical stages (Figure 4), i.e., (1) original microcrack closure; (2) elastic deformation; (3) sudden stress drop; and (4) residual behavior.

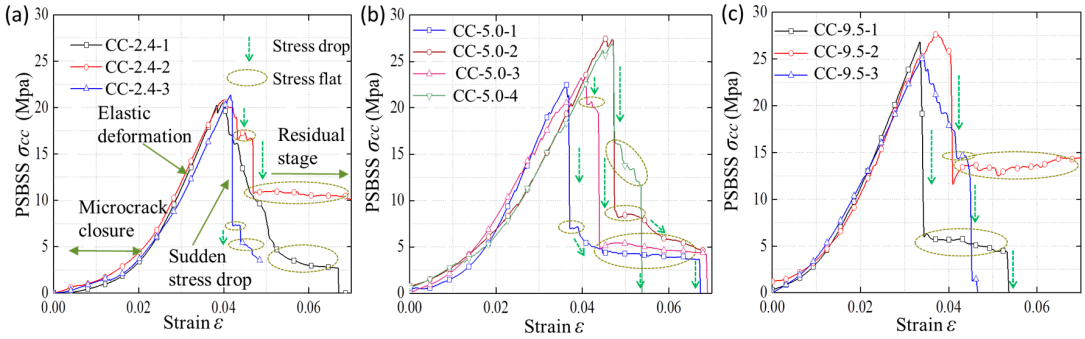

Figure 4. Typical plane-strain biaxial stress-strain curves. (**a**) Stress-strain curves at a strain rates of 2.4×10^{-4}/s; (**b**) Stress-strain curves at a strain rates of 5.0×10^{-4}/s; (**c**) Stress-strain curves at a strain rates of 9.5×10^{-4}/s.

Prior to the peak, two stages (i.e., microcrack closure and elastic deformation stages) can be identified. During the stage of sealing (microcrack closure), the PSBSS compression stress-strain curve of the coal sample is a downward concave shape, which may result from the closure of some primary pores and voids in the sample with the increasing compression stress. Korinets and Alehossein [37] suggested that interface-imperfection effects can also dominate the initial downward concave (or non-linear deformation) nature of the strain-stress curve. However, for brittle coal with a higher porosity compared with rocks such as granite, the closure of some primary pores and voids would be a dominant reason for the formation of the non-linear deformation. Moreover, the rigidity of the coal sample at the initial stage of deformation has a better consistency and is not dependent on the strain rates. During the stage of elastic deformation, the loading begins with the increase of axial stress, and elastic deformation dominates the stress-strain curve of the coal samples. The linear stress-strain behavior of the sample does not change, although there are some irrecoverable processes at this stage, such as crack initiation. At the end of the elastic deformation, the peak strength is attained, followed by the post-peak behavior.

During the post-peak stage, with the generation and coalescence of cracks, a sudden stress drop occurs, which is followed by strain-softening behaviors that may be caused by the friction of fissure surfaces. Interestingly, the sudden stress drop occurs in a multistage manner, i.e., a stress drop is often followed by a 'stress flat' (indicated by circle in Figure 4). After the 'stress flat' behaviors, new cracks rapidly form, and the strength behavior in the stress-strain curves shows another rapid drop. It was revealed that the residual stage performs well at a certain confined stress, and the confined stress (σ_2) had a pronounced effect on the failure strength [38] of geomaterials. Specifically, the peak stress and peak strain under biaxial compression was greater than that under uniaxial compression [27–29]. In our PSBSS test results, the residual stage is remarkable, which may also result from the confined pressure (σ_2) that is provided by the vertical walls. Although the residual stages varied, especially in Figure 4a,c, the post-peak behavior in the PSBSS tests can be considerable.

3.1.2. Effect of the Strain Rate on Peak Strength

It was revealed that the strength of rock is affected by the axial strain rate or stress rate [39,40]. In addition, a higher strain rate indicates a greater peak strength [41–43]. Figure 5 indicates that the strain rates have a significant effect on the strength of coal samples under the PSBSS compression. In accordance with previous studies, the peak strain increases with the rise of the strain rate in the PSBSS compression test. By increasing the strain rate from 2.4×10^{-4}/s to 9.0×10^{-4}/s, the peak strength under PSBSS compression increased from 21.04 MPa to 26.68 MPa.

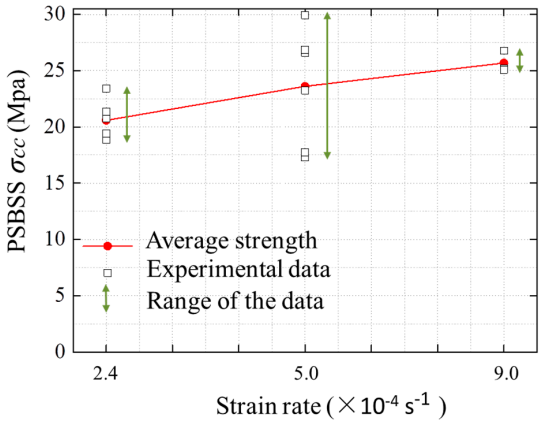

Figure 5. Effect of strain rates on peak strength of coal specimens under PSBSS compression.

It is well known that rock is a typical non-homogeneous material which may contain fractures, microcracks, pores, and voids. These flaws can, to a greater or lesser degree, affect the strength and deformation behavior of rock [40]. As mentioned in Section 2.1, inner-natural flaws are inevitable, even though the coal specimens were carefully selected. The experimental error at a strain rate of 5.0×10^{-4}/s is relatively high. Particularly, the minimum failure strength is 17.29 MPa, while the maximum strength is 29.94 MPa (see Table 2 for more details). This error may result from the non-homogeneity of coal specimens and the flaw distribution in the coal specimens.

3.1.3. Failure Patterns of Coal Specimens

The crack patterns and failure modes for all of the coal cubes were analyzed. Figure 6 shows typical photographs of the failure modes that were observed under PSBSS compression. In general, the failure modes are similar. Because the effective measures of friction-reduction were employed (i.e., lube oil), all of the cubes under PSBSS compression became column-type fragments, and the cracks were basically parallel to the applied load.

Interestingly, for coal specimens subjected to the PSBSS test, the generated cracks are perpendicular to the vertical walls. This indicates that coal specimens trend toward bursting through

the unconfined surfaces layer by layer under the PSBSS compression. This phenomenon is similar to coal bump [44]. Moreover, the cracks are much more parallel to the applied load with a greater strain rate. As shown in Figure 6(a-2,b-2,c-2), it seems that shear-type failure tended to form with a relatively low strain rate, such as a strain rate lower than 2.4×10^{-4}/s, while when the strain rate increased to 5.0×10^{-4}/s or 9.5×10^{-4}/s in Figure 6b,c, the parallel plate-type fragments were more prominent. The center area is relatively stable without explosion, which is helpful for attaining a residual strength, even though the free sides were crushed into fragments.

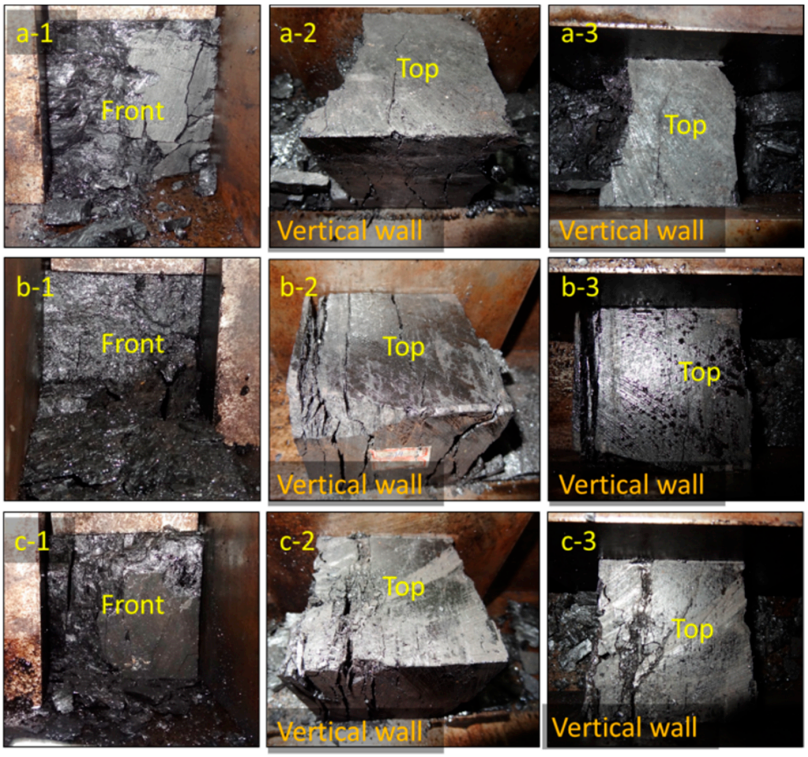

Figure 6. Failure modes of the coal specimens subjected to the plane-strain biaxial compression. (**a**) Failure modes of a specimen with a strain rate of 2.4×10^{-4}/s; (**a-1**) Front surface (free face) (**a-2**) Oblique picture (**a-3**) Top surface (loading face); (**b**) Failure modes of a specimen with a strain rate of 5.0×10^{-4}/s; (**c**) Failure modes of a specimen with a strain rate of 9.5×10^{-4}/s.

3.2. Mechanical and Deformation Behavior of Synthetic Specimens under PSBSS Compresiion

The strength and deformation behavior of the brittle specimens (coal) were obtained and analyzed. However, the rock mass or ductile rock usually experience a ductile yield instead of a brittle rupture after the peak strength. Thus, the axial stress-strain behavior and deformation characterization of the synthetic specimens under the PSBSS are illustrated.

3.2.1. Stress-Strain Curves of Synthetic Specimens

Figure 7 presents the stress-strain curves of the synthetic specimens under the PSBSS compression tests. Prior to the peak, the initial microcrack closure and elastic deformation stage can be identified as the start of loading with the increase of axial stress, and at the end of the elastic deformation, the curves reach peak strengths. In the post-peak stage, strain-softening behavior and a residual stage can be easily identified. Similar to the stress-strain behavior of the coal specimens, the initial microcrack stage can be identified as having a downward concave shape. However, this stage is difficult to observe due to the synthetic specimens being relatively homogenous and a prepressing method was employed to reduce the primary pores and voids in the specimens during the preparation of the material.

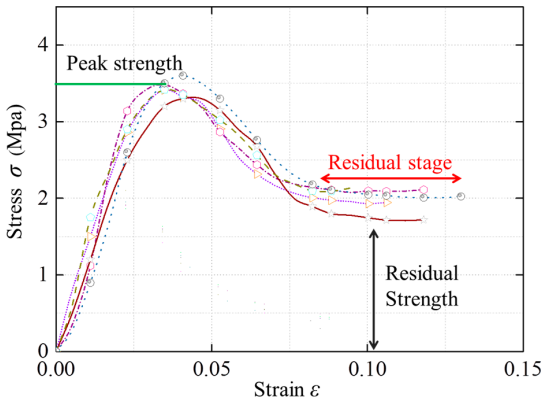

Figure 7. Stress-strain curves of synthetic specimens under PSBSS compression.

The stress experienced a moderate drop after the peak strength was exceeded, which is different from the periodic stress drop in the curve of the coal specimens. This may be because the synthetic material is ductile and can absorb the energy induced by compressed deformation. The residual stages in the synthetic specimen are remarkable and consistent with each other, which in turn verifies the homogeneity of our synthetic materials and confirms that the experimental apparatus has little influence on the test data error. Previous studies also presented a noticeable residual strain range of sand specimens [33]. The residual loading capacity in our study can be explained by the stable zone formed in the center (Figure 8), which is the result of a shear-type failure.

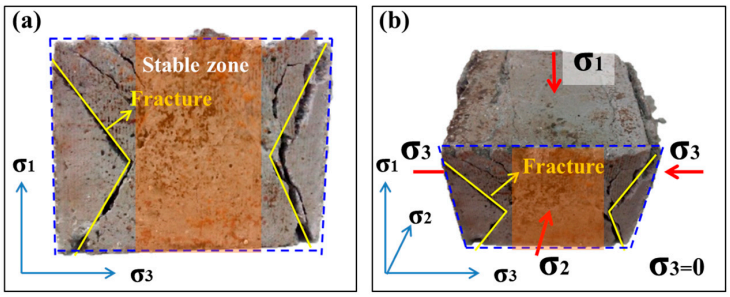

Figure 8. Failure modes of synthetic specimens subjected to the plane-strain biaxial compression. (**a**) Confined face, i.e., the face against the vertical wall; (**b**) Oblique picture of the PSBSS compression.

3.2.2. Failure Patterns of Synthetic Specimens

Shear-type failures are generally observed in the PSBSS tests of synthetic specimens. An 'X'-like failure shape divided the specimen into three parts, and a stable zone formed in the middle (Figure 8). Although these specimens were compressed to a residual stage, they can keep stable with the existing of this stable zone. Powrie et al. [33] and Alshibli et al. [34] found similar failure shapes in Ottawa sand and numerical samples, respectively. Powrie et al. defined this failure pattern as 'conjugate shear bands'. However, this failure mode is unavailable in the brittle rocks that have been illustrated in Figure 6.

In an underground mining system, a coal pillar is retained to support the overlying strata. Zheng et al. [45] revealed that the vertical stress distribution along the *y*-axial direction (Figure 1) in the coal pillar is unimodal. Wang et al. [6] explored the dynamic mechanical state of a coal pillar and suggested that an elastic core exists in the center, indicating that this core plays a significant role in the loading capacity of the zone. By employing electronic peering instruments to detect the deformation of the long pillar in the in situ 6302 working face in the Baodian coalmine, Zhang et al. [46] found that the pillar can be divided into three zones along the *y*-axial direction (Figure 1), namely the fracture

zone, stable zone, and collapsed zone, suggesting that the stable zone in the middle of the pillar is key to the stability of the coal pillar. The results of the previous studies correspond to the failure pattern of the coal and synthetic specimens in this study.

3.3. Failure Criteria

3.3.1. Stress Strain Relationship under the PSBSS

It is well known that failure often occurs at peak strength or is initiated at peak strength [9]. According to the generalized Hook's law, the stress-strain relationship for isotropic elasticity and complete plane strain can be determined by principle stresses and is described as:

$$\sigma_1 = E\varepsilon_1 / \left(1 - \mu^2\right) \quad (1)$$

where σ_1, E, ε_1, and μ are the maximum principle stress, elastic modulus, maximum principle strain, and Poisson's ratio, respectively. The intermediate principle stress σ_2 corresponds to the maximum σ_2, and $\sigma_2 = \mu\sigma_1$.

3.3.2. Strength Coefficient

The failure strength of a specimen can be enhanced by applying a confined stress. Thus, the PSBSS peak strength is greater than the uniaxial compression strength and the test results are listed in detail in Table 2. In the uniaxial tests, the intermediate principle stress (σ_2) is zero. We defined a strength coefficient ($K > 1.0$), a ratio of the PSBSS peak strength (σ_{cc}) to uniaxial compression strength (σ_c) (see Table 2), to illustrate the strengthening effect of the PSBSS with respect to a uniaxial stress state. According to the Mohr-Coulomb criterion, there is a linear correlation between peak strength and confined pressure [47]. Thus, the strength coefficient may be solved by introducing competent failure criteria that consider the intermediate principle stress, which will be discussed in the following section.

Table 2. Experimental results of the coal and synthetic specimens in the PSBSS and uniaxial compression tests.

Coal Specimens							
Strain Rate (10^{-4}/s)	**Specimen Number**	**PSBSS Test**		**Specimen Number**	**Uniaxial Test (σ_2 = 0)**		**Strength Coefficient**
		Peak Strength (MPa)			**Peak Strength (MPa)**		
		Individial Value	**Average Value**		**Individial Value**	**Average Value**	
2.4	CC-2.4-1	20.58	21.04	C-2.4-1	18.84	18.84	1.12
	CC-2.4-2	21.27		C-2.4-2	19.00		
	CC-2.4-3	20.73		C-2.4-3	17.65		
	CC-2.4-4	18.87		C-2.4-4	19.86		
	CC-2.4-5	23.40					
	CC-2.4-6	21.35					
5.0	CC-5.0-1	23.61	23.89	C-5.0-1	20.12	20.12	1.19
	CC-5.0-2	26.59		C-5.0-2	18.74		
	CC-5.0-3	26.86		C-5.0-3	20.27		
	CC-5.0-4	23.25		C-5.0-4	21.36		
	CC-5.0-5	19.75					
	CC-5.0-6	29.94					
	CC-5.0-7	17.29					
9.5	CC-9.5-1	25.68	26.68	C-9.5-1	23.00	23.00	1.16
	CC-9.5-2	25.08		C-9.5-2	22.70		
	CC-9.5-3	27.18		C-9.5-3	21.03		
	CC-9.5-4	28.77		C-9.5-4	25.26		
Synthetic materials							
2.4	CC-1	3.50	3.45	C-1	2.10	2.10	1.64
	CC-2	3.48		C-2	2.20		
	CC-3	3.30		C-3	1.90		
	CC-4	3.35		C-4	2.10		
	CC-5	3.60		C-5	2.18		

3.3.3. Criteria Study

To estimate the peak strength under the PSBSS and the strength coefficient (K), we conducted a criteria study, including von Mises, Drucker-Prager, Modified Wiebols-Cook, and Modified Lade criteria which consider the middle principle stress. According to the testing method recommended by the International Society for Rock Mechanics Committee [48], the Poison's ratios of coal and synthetic materials are identified as 0.3 and 0.32, respectively. The internal friction angle of the coal and synthetic material was determined as 25 degrees and 45 degrees, respectively. The results of the theoretical solutions and values are shown in Table 3.

Table 3. Results of the strength coefficient under different criteria.

Failure Criteria	Strength Coefficient Function ($K = \sigma_{cc}/\sigma_c$)	K-Coal	K-Synthetic
von Mises criterion	$K = 1/\sqrt{1-u+u^2}$	1.125	1.131
Drucker-Prager criterion [49]	$K = \left(\alpha+\sqrt{3}\right)\Big/\left[\alpha(1+u)+\sqrt{3(1-u+u^2)}\right]$ $\alpha = 2\sin\varphi\Big/\left[\sqrt{3}(3-\sin\varphi)\right]$ $k = 6c\sin\varphi\Big/\left[\sqrt{3}(3-\sin\varphi)\right]$	1.076	1.043
Modified Wiebols-Cook criterion [50]	$\begin{cases}\frac{[(\sigma_c+S)+2S)]^3}{(\sigma_c+S)S^2} = 27+\frac{4\tan^2\varphi(9-7\sin\varphi)}{1-\sin\varphi}\\ \frac{[(1+u)\sigma_{cc}+3S]^3}{(\sigma_{cc}+S)(u\sigma_{cc}+S)S} = 27+\frac{4\tan^2\varphi(9-7\sin\varphi)}{1-\sin\varphi}\end{cases}$ $S = c/\tan\varphi$ $K = \sigma_{cc}/\sigma_c$	1.344	1.785
Modified Lade criterion [51]	$K = \frac{2C\left\{\begin{array}{l}\sqrt{3}\sqrt{1+\mu^2}-\mu-B(1+\mu)-\\ \sqrt{\left[B(1+\mu)-\sqrt{3}\sqrt{1+\mu^2}-\mu\right]^2-4AC(1+\mu)^2}\end{array}\right\}}{\left[2C(1+\mu)^2/3\right]\left[3\left(\sqrt{3}-B\right)-3\sqrt{\left(B-\sqrt{3}\right)^2-4AC}\right]}$ $A = \sigma_c/\sqrt{3}-\sigma_c B/3-{\sigma_c}^2C/9$ $C = \frac{\sqrt{27}}{2C_1-\sigma_c}\left(\frac{C_1-\sigma_c}{2C_1-\sigma_c}-\frac{q-1}{q+2}\right)$ $B = \sqrt{3}(q-1)/(q+2)-2C\sigma_c/3$ $q = \tan^2(\pi/4+\varphi/2)$	1.314	1.741

Note that K is the strengthen coefficient, σ_c and σ_{cc} are the uniaxial compression strength and the PSBSS strength, respectively. c is the cohesive strength, μ is Poison's ratio, and φ is the internal friction angle. Particularly, cohesive strength is not related with the strength coefficient K.

We plot the theoretical curves and experimental data in Figure 9. It is clear that for the coal specimen, the theoretical results achieve a good fit with the test data under the von Mises criterion (Figure 9a), while for the synthetic materials, the test data is greater than the theoretical data: 1.640 versus 1.131. Moreover, the strength coefficient K only depends on the Poison's ratio. In Figure 9b–d, the theoretical curves for the coal specimen (internal friction angle is 25°) and synthetic materials (internal friction angle is 45°) are presented with Drucker-Prager, Modified Wiebols-Cook, and Modified Lade criteria, respectively. The results under the Drucker-Prager criterion are similar to the von Mises criterion. Figure 9c,d show that the experimental data of the synthetic specimens fit well with the theoretical curves. However, the rock data is lower than the theoretical value under the Modified Wiebols-Cook and Modified Lade criteria. With the increase of the internal friction angle, this coefficient was raised, and with a higher internal friction angle, the effects of the Poison's ratio on peak strength are much stronger.

A decrease in rock strength recorded with an increase of microcracks is a well-known phenomenon in rock mechanics. In coal, natural flaws play an important role in reducing coal strength [52] and the theoretical value of the strength coefficient may be, to a greater or lesser extent, greater than that of the real sample which contains microcracks or fissures. For synthetic materials, which are encased in a homogenous manner, the experimental value should be closer to the theoretical data. In this way, the Modified Lade and Modified Wiebols-Cook criteria are qualified to estimate the PSBSS peak strength.

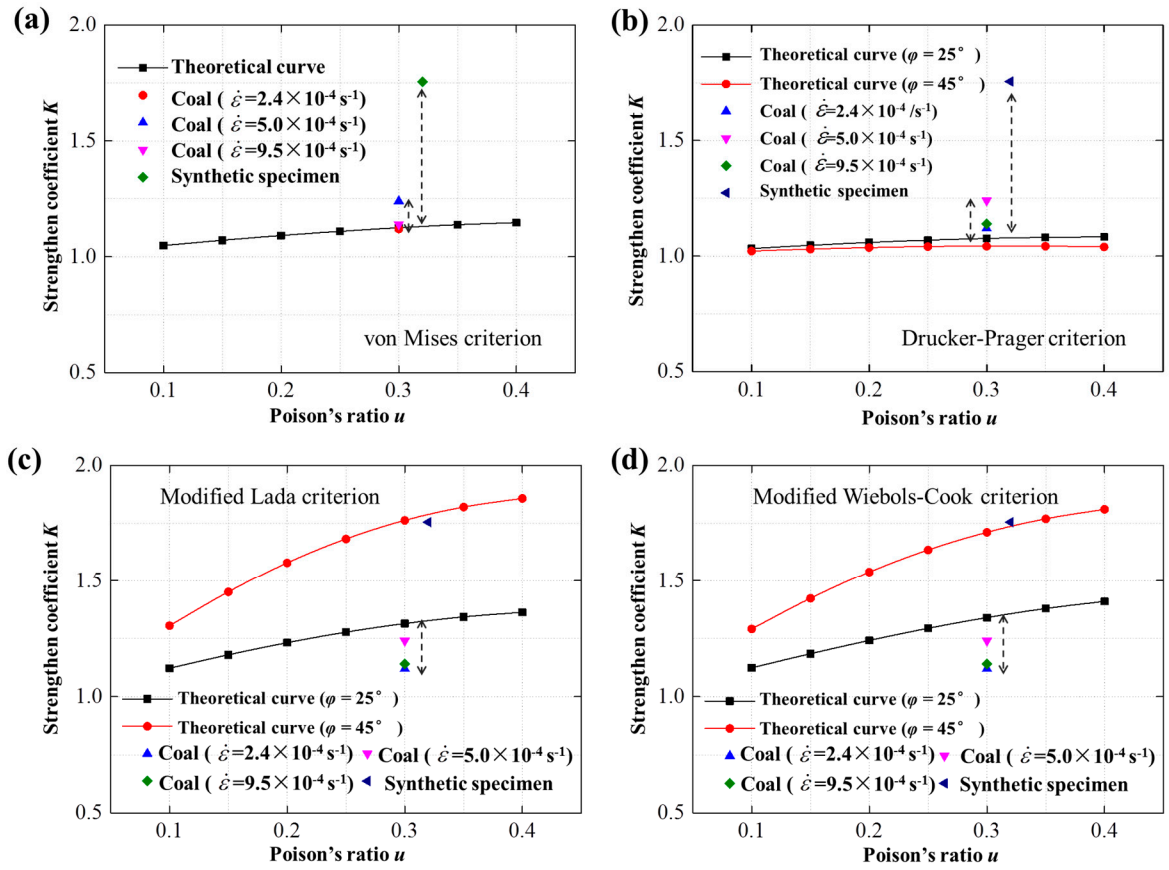

Figure 9. Relationship between strength coefficient K and Poisson's ratio under four criteria. (**a**) Von Mises criterion; (**b**) Drucker-Prager criterion; (**c**) Modified Lade criterion; (**d**) Modified Wiebols-Cook criterion. In (**b**–**d**), curves are plotted with the internal friction angle φ.

4. Conclusions

An experimental investigation on the strength behavior and failure mode of coal (brittle) and synthetic samples (ductile) under plane-strain biaxial compression was performed. On the basis of the experimental results and theoretical analysis, the following conclusions can be drawn.

(1) The stress-strain curves of the coal and synthetic specimens under the PSBSS can be divided into four typical stages, namely original microcrack closure, elastic deformation, sudden stress drop, and residual behavior. The stress-strain curve of coal under PSBSS compression showed periodic stress drops during the post-peak phase, that is, the stress decreased dramatically while the strain decreased slowly. The curve of the synthetic specimen presented a moderate decrease during the post-peak stage. Obvious residual strengths of coal and composites can be observed in these curves, which is vital to the stability of specimens after the failure strength is exceeded.

(2) Strain rates have a significant effect on the strength of coal samples under PSBSS compression. Specifically, the compressive stress increased with the increase of the strain rate.

(3) During PSBSS compressive tests, coal showed a split failure. A conjugate shear failure pattern can be identified for the synthetic materials. Interestingly, the central region is more stable than both sides of the coal and composites after PSBSS compression. The formation of the stable region was caused by blinding from a lateral plate, and the stable region played an important role in forming the residual strength after PSBSS compression tests.

(4) The failure criterion considering the intermediate principal stress can be used to estimate the strength coefficient of the coal and composite material under PSBSS compression, and the coefficient is the ratio of PSBSS peak strength to uniaxial compressive strength. Through the

comparative analysis of the failure criteria, it can be concluded that The Modified Lade and Modified Wiebols-Cook criteria are competent to estimate the PSBSS peak strength.

Acknowledgments: This work was supported by the National Natural Science Foundation of China (grant numbers: 51674242 and 51604267).

Author Contributions: Hongwei Zhang and Zhijun Wan conceived and designed the experiments; Hongwei Zhang, Zhijun Wan, and Yuan Zhang performed the experiments; Hongwei Zhang, Dan Ma and Jingyi Cheng analyzed the data; Hongwei Zhang, Dan Ma, and Qi Zhang wrote the paper.

Conflicts of Interest: The authors declare no conflict of interest.

References

1. Hoek, E.; Brown, E. Practical Estimates of Rock Mass Strength. *Int. J. Rock Mech. Min. Sci.* **1997**, *34*, 1165–1186. [CrossRef]
2. Shou, K.J. A Three-Dimensional Hybrid Boundary Element Method for Non-Linear Analysis of a Weak Plane near an Underground Excavation. *Tunn. Undergr. Space Technol.* **2000**, *15*, 215–226. [CrossRef]
3. Akhlaghi, Y.G.; Tureyen, O.I.; Satman, A. Modeling the Temperature Behavior of Ground Source Heat Pump Systems. In Proceedings of the 41th Stanford Geothermal Workshop, Stanford, CA, USA, 22–24 February 2016; pp. 1–11.
4. Soderman, K.L.; Giroud, J.P. Relationships between Uniaxial and Biaxial Stresses and Strains in Gepsunthetics. *Geosynth. Int.* **1995**, *2*, 495–504. [CrossRef]
5. Gao, F.; Kang, H. Experimental Study on the Residual Strength of Coal under Low Confinement. *Rock Mech. Rock Eng.* **2017**, *50*, 285–296. [CrossRef]
6. Wang, H.; Jiang, Y.; Zhao, Y.; Zhu, J.; Liu, S. Numerical Investigation of the Dynamic Mechanical State of a Coal Pillar during Longwall Mining Panel Extraction. *Rock Mech. Rock Eng.* **2013**, *46*, 1211–1221. [CrossRef]
7. Zipf, R.K. Ground Control Design for Highwall Mining. In Proceedings of the 2005 SME Annual Meeting, Salt Lake City, UT, USA, 28 February–2 March 2005.
8. Adhikary, D.P.; Shen, B.; Fama, M.E.D. A Study of Highwall Mining Panel Stability. *Int. J. Rock Mech. Min. Sci.* **2002**, *39*, 643–659. [CrossRef]
9. Brady, B.H.G.; Bray, J.W. The Boundary Element Method for Determining Stresses and Displacements around Long Openings in a Triaxial Stress Field. *Int. J. Rock Mech. Min. Sci. Geomech. Abstr.* **1978**, *15*, A103. [CrossRef]
10. Kupfer, H.; Hilsdorf, H.K.; Rusch, H. Behavior of Concrete under Biaxial Stresses. *J. Proc.* **1969**, *66*, 656–666.
11. Mogi, K. Effect of the Intermediate Principal Stress on Rock Failure. *J. Geophys. Res.* **1967**, *72*, 5117–5131. [CrossRef]
12. Basheeev, G.V.; Martynyuk, P.A.; Sher, E.N. Statistical Modeling of Rock Failure under Biaxial Compression.Part I: Shear Crack Interaction. *J. Min. Sci.* **2003**, *39*, 467–474. [CrossRef]
13. Mokni, M.; Desrues, J. Strain Localization Measurements in Undrained Plane-Strain Biaxial Tests on Hostun RF Sand. *Mech. Cohes.-Frict. Mater.* **1999**, *4*, 419–441. [CrossRef]
14. Wang, H.L.; Song, Y.P. Biaxial Compression Behaviour of Different Aggregate Graded Concrete. *Mag. Concr. Res.* **2009**, *61*, 457–463. [CrossRef]
15. Kulatilake, P.H.S.W.; Park, J.; Malama, B. A New Rock Mass Failure Criterion for Biaxial Loading Conditions. *Geotech. Geol. Eng.* **2006**, *24*, 871–888. [CrossRef]
16. Makhnenko, R.; Labuz, J. Plane Strain Testing with Passive Restraint. *Rock Mech. Rock Eng.* **2013**, *47*, 2021–2029. [CrossRef]
17. Wiebols, G.A.; Cook, N.G.W. An Energy Criterion for the Strength of Rock in Polyaxial Compression. *Int. J. Rock Mech. Min. Sci.* **1968**, *5*, 529–549. [CrossRef]
18. Hussein, A.A. *Behaviour of High-Strength Concrete under Biaxial Loading Conditions*; Memorial University of Newfoundland: St. John's, NL, Canada, 1998.
19. Haimson, B.; Chang, C. A New True Triaxial Cell for Testing Mechanical Properties of Rock, and Its Use to Determine Rock Strength and Deformability of Westerly Granite. *Int. J. Rock Mech. Min. Sci.* **2000**, *37*, 285–296. [CrossRef]

20. Linse, D.; Kesler, C.E. Strength of Concrete under Biaxial Sustained Load. In *International Seminar on Concrete for Nuclear Reactors*; American Concrete Institute: Detroit, AL, USA, 1972; Volume 1.
21. He, Z.; Song, Y. Failure Mode and Constitutive Model of Plain High-Strength High-Performance Concrete under Biaxial Compression after Exposure to High Temperatures. *Acta Mech. Solida Sin.* **2008**, *21*, 149–159. [CrossRef]
22. Ehm, E.; Schneider, U. The High Temperature Behavior of Concrete under Biaxial Conditions. *Cem. Concr. Res.* **1985**, *15*, 27–34. [CrossRef]
23. Li, J. Experimental Study on RCC under Biaxial Compression. *J. Hrdraul. Eng.* **2000**, *31*, 29–32.
24. Liu, T.C.Y.; Nilson, A.H.; Floyd, F.O.S. Stress-Strain Response and Fracture of Concrete in Uniaxial and Biaxial Compression. *J. Proc.* **1972**, *69*, 291–295.
25. Song, Y.; Zhao, G. Behavior of Deformation and Strength of Concrete under Baxial Stresses. *China Ocean Eng.* **1991**, *5*, 347–360.
26. Tasuji, M.E.; Nilson, A.H. Stress-Strain Response and Fracture of Concrete in Biaxial Loading. *J. Proc.* **1978**, *75*, 306–312.
27. Sahouryeh, E. Crack Growth under Biaxial Compression. *Eng. Fract. Mech.* **2002**, *69*, 2187–2198. [CrossRef]
28. Liu, L.; Tang, D.; Zhai, X. Failure Criteria for Grouted Concrete Block Masonry under Biaxial Compression. *Adv. Struct. Eng.* **2006**, *9*, 229–240. [CrossRef]
29. Lim, D.H.; Nawy, E.G. Behaviour of Plain and Steel-Fibre-Reinforced High-Strength Concrete under Uniaxial and Biaxial Compression. *Mag. Concr. Res.* **2005**, *57*, 603–610. [CrossRef]
30. Labuz, J.F.; Dai, S.-T.; Papamichos, E. Plane-Strain Compression of Rock-like Materials. *Int. J. Rock Mech. Min. Sci. Geomech. Abstr.* **1996**, *33*, 573–584. [CrossRef]
31. Papamichos, E.; Labuz, J.F.; Vardoulakis, I. A Surface Instability Detection Apparatus. *Rock Mech. Rock Eng.* **1994**, *27*, 37–56. [CrossRef]
32. Tao, Z. *Theory and Practice of Rock Mechanics*; Wuhan University: Wuhan, China, 2013.
33. Powrie, W.; Ni, Q.; Harkness, R.M.; Zhang, X. Numerical Modelling of Plane Strain Tests on Sands Using a Particulate Approach. *Geotechnique* **2005**, *55*, 297–306. [CrossRef]
34. Alshibli, K.A.; ASCE, M.; Batisete, S.N.; Sture, S. Strain Localization in Sand: Plane Strain versus Triaxial Compression. *J. Geotech. Geoenviron. Eng.* **2003**, *129*, 483–494. [CrossRef]
35. Li, H. *Experimental Simulation of Mine Ground Pressure*; China University of Mining & Technology Press: Xuzhou, China, 1988.
36. Ince, N.; Kao, C.; Kaveh, M.; Tewfik, A.; Labuz, J. A Machine Learning Approach for Locating Acoustic Emission. *EURASIP J. Adv. Signal Process.* **2010**, *2010*, 1–14. [CrossRef]
37. Korinets, A.; Alehossein, H. On the Initial Non-Linearity of Compressive Stress-Strain Curves for Intact Rock. *Rock Mech. Rock Eng.* **2002**, *35*, 319–328. [CrossRef]
38. Yang, S.Q.; Jiang, Y.Z.; Xu, W.Y.; Chen, X.Q. Experimental Investigation on Strength and Failure Behavior of Pre-Cracked Marble under Conventional Triaxial Compression. *Int. J. Solids Struct.* **2008**, *45*, 4796–4819. [CrossRef]
39. Sano, O.; Ito, I.; Terada, M. Influence of Strain Rate on Dilatancy and Strength of Oshima Granite under Uniaxial Compression. *J. Geophys. Res. Solid Earth* **1981**, *86*, 9299–9311. [CrossRef]
40. Bieniawski, Z.T. The Effect of Specimen Size on Compressive Strength of Coal. *Int. J. Rock Mech. Min. Sci.* **1968**, *5*, 325–335. [CrossRef]
41. Olsson, W.A. The Compressive Strength of Tuff as a Function of Strain Rate from 10^{-6}, to 10^{3}/sec. *Int. J. Rock Mech. Min. Sci.* **1991**, *28*, 115–118. [CrossRef]
42. Lankford, J. Mechanisms Responsible for Strain-Rate-Dependent Compressive Strength in Ceramic Materials. *J. Am. Ceram. Soc.* **1981**, *64*, C-33–C-34. [CrossRef]
43. Lajtai, E.Z.; Duncan, E.J.S.; Carter, B.J. Technical Note—The Effect of Strain Rate on Rock Strength. *Rock Mech. Rock Eng.* **1991**, *24*, 99–109. [CrossRef]
44. He, M.C.; Miao, J.L.; Feng, J.L. International Journal of Rock Mechanics & Mining Sciences Rock Burst Process of Limestone and Its Acoustic Emission Characteristics under True-Triaxial Unloading Conditions. *Int. J. Rock Mech. Min. Sci.* **2010**, *47*, 286–298.
45. Zheng, X.; Yao, Z.; Zhang, N. Stress Distribution of Coal Pillar with Gob-Side Entry Driving in the Process of Excavation and Mining. *J. Min. Saf. Eng.* **2012**, *29*, 459–465.

46. Zhang, H.; Wan, Z.; Zhang, Y.; Ma, Z.; Zhang, J.; Ge, L. Deformation Mechanism of Narrow Coal Pillar in the Fully-Mechanized Gob-Side Entry with Incompletely Stable Overlying Strata. *J. Min. Saf. Eng.* **2016**, *33*, 692–698.
47. Rummel, F.; Fairhurst, C. Determination of the Post-Failure Behavior of Brittle Rock Using a Servo-Controlled Testing Machine. *Rock Mech. Rock Eng.* **1970**, *2*, 189–204. [CrossRef]
48. Bieniawski, Z.T.; Bernede, M.J. Suggested Methods for Determining the Uniaxial Compressive Strength and Deformability of Rock Materials: Part 1. Suggested Method for Determining Deformability of Rock Materials in Uniaxial Compression. *Int. J. Rock Mech. Min.* **1970**, *16*, 138–140. [CrossRef]
49. Drucker, D.C.; Prager, W. Soil Mechanics and Plastic Analysis or Limit Design. *Q. Appl. Math.* **1952**, *10*, 157–165. [CrossRef]
50. Ewy, R.T. Wellbore-Stability Predictions by Use of a Modified Lade Criterion. *SPE Drill. Complet.* **1999**, *14*, 85–91. [CrossRef]
51. Zhou, S. A Program to Model the Initial Shape and Extent of Borehold Breakout. *Comput. Geosci.* **1994**, *20*, 1143–1160. [CrossRef]
52. Poulsen, B.A.; Adhikary, D.P. A Numerical Study of the Scale Effect in Coal Strength. *Int. J. Rock Mech. Min. Sci.* **2013**, *63*, 62–71. [CrossRef]